Visualizing context-dependent calcium signaling in encephalitogenic T cells in vivo by two-photon microscopy

Nikolaos I. Kyratsous[a,b], Isabel J. Bauer[a,b], Guokun Zhang[a], Marija Pesic[a,b], Ingo Bartholomäus[b], Marsilius Mues[b], Ping Fang[a,b], Miriam Wörner[a], Stephanie Everts[a], Joachim W. Ellwart[c], Joanna M. Watt[d,e], Barry V. L. Potter[e], Reinhard Hohlfeld[a,f], Hartmut Wekerle[b,f,1], and Naoto Kawakami[a,b,1]

[a]Institute of Clinical Neuroimmunology, University Hospital and Biomedical Center, Ludwig-Maximilians University Munich, 81377 Munich, Germany; [b]Neuroimmunology Group, Max Planck Institute of Neurobiology, 82152 Martinsried, Germany; [c]Institute for Experimental Hematology, Helmholtz Center, 81377 Munich, Germany; [d]Wolfson Laboratory of Medicinal Chemistry, Department of Pharmacy and Pharmacology, University of Bath, Bath, BA2 7AY, United Kingdom; [e]Medicinal Chemistry and Drug Discovery, Department of Pharmacology, University of Oxford, Oxford OX1 3QT, United Kingdom; and [f]Munich Cluster for Systems Neurology (SyNergy), Ludwig-Maximilians University Munich, 81377 Munich, Germany

Edited by Lawrence Steinman, Stanford University School of Medicine, Stanford, CA, and approved June 21, 2017 (received for review February 2, 2017)

In experimental autoimmune encephalitis (EAE), autoimmune T cells are activated in the periphery before they home to the CNS. On their way, the T cells pass through a series of different cellular milieus where they receive signals that instruct them to invade their target tissues. These signals involve interaction with the surrounding stroma cells, in the presence or absence of autoantigens. To portray the serial signaling events, we studied a T-cell–mediated model of EAE combining in vivo two-photon microscopy with two different activation reporters, the FRET-based calcium biosensor Twitch1 and fluorescent NFAT. In vitro activated T cells first settle in secondary (2°) lymphatic tissues (e.g., the spleen) where, in the absence of autoantigen, they establish transient contacts with stroma cells as indicated by sporadic short-lived calcium spikes. The T cells then exit the spleen for the CNS where they first roll and crawl along the luminal surface of leptomeningeal vessels without showing calcium activity. Having crossed the blood–brain barrier, the T cells scan the leptomeningeal space for autoantigen-presenting cells (APCs). Sustained contacts result in long-lasting calcium activity and NFAT translocation, a measure of full T-cell activation. This process is sensitive to anti-MHC class II antibodies. Importantly, the capacity to activate T cells is not a general property of all leptomeningeal phagocytes, but varies between individual APCs. Our results identify distinct checkpoints of T-cell activation, controlling the capacity of myelin-specific T cells to invade and attack the CNS. These processes may be valuable therapeutic targets.

autoimmunity | intracellular calcium | T-cell activation | central nervous system | two-photon imaging

The tissues of the CNS are secluded from the circulating blood by a complex cerebrovascular wall system, the blood–brain barrier (BBB) (1). Although holding back most blood-borne macromolecules and cells, the BBB allows access to a highly selected set of blood components. These components include specialized immune cells that are required for immune surveillance of the tissues, but also encephalitogenic immune cells that mediate brain disease, such as multiple sclerosis (2, 3).

Encephalitogenic T cells take a complicated path to reach the CNS. After activation in a remote peripheral site, such as in the intestine (4), they first spend a brief time in secondary (2°) lymphatic organs and then cross the endothelial BBB and finally reach their ultimate destination, the CNS white matter. In the lymph nodes, lung, and spleen, freshly activated T cells acquire a functional phenotype that enables them to successfully overcome the cerebrovascular BBB (5, 6). Beyond the vascular barrier, the T cells are confronted with phagocytes that, by presenting myelin autoantigen, usher them into the compact CNS white matter (7–9). This itinerary implies that the autoimmune T cell drifts sequentially through different milieus where it interacts with diverse local stroma structures through intercellular membrane contacts and/or soluble signals in the presence or absence of autoantigens.

Many of the signals that influence T-cell functions involve immediate changes in the intracellular calcium level. The profiles and amplitudes of these oscillations define the characteristics of the consequent cellular response (10). In this study, we used a functional fluorescent indicator to track the calcium activity of encephalitogenic T cells on their way from the peripheral immune system into the CNS white matter.

We used a modified version of the calcium indicator Twitch1, a fluorescence resonance energy transfer (FRET)-based reporter protein (11) that is expressed by retroviral gene transfer (12) in rat encephalitogenic T cells (13). To correlate calcium changes with the activation events downstream of calcium signaling, we followed the calcium-dependent nuclear translocation of a truncated Nuclear Factor of Activated T Cells (NFAT)–GFP fusion protein (8, 14, 15).

We report that in autoantigen-free milieus of peripheral lymphoid organs, T cells respond with chemokine-dependent acute calcium signaling, which is not followed by NFAT translocation. In contrast, after passing through the BBB, in the leptomeningeal and spinal cord parenchymal compartments, the T cells establish contacts with individual autoantigen-presenting cells (APCs) that result in sustained calcium plateaus and followed by NFAT translocation into the nucleus. Our observations define context-dependent serial checkpoints along the migration of encephalitogenic T cells into the CNS. Each of these checkpoints significantly influences T-cell fate and migratory behavior. Because these processes are essential

Significance

Before invading the central nervous system, encephalitogenic T cells cross a series of microenvironments where they interact with local cells. T-cell activation was visualized by specific calcium signals using a combination of a genetic calcium reporter, Twitch1, and in vivo two-photon microscopy. In peripheral immune organs, short-lived calcium signaling indicated antigen-independent interactions. By contrast, in the CNS, saturated long-lived calcium signaling was induced by endogenous autoantigens presented by a subset of local antigen-presenting cells. Because T-cell trafficking is controlled at serial checkpoints, our findings may help to identify therapeutic targets for preventing CNS inflammation.

Author contributions: H.W. and N.K. designed research; N.I.K., I.J.B., M.P., M.M., M.W., S.E., J.W.E., and N.K. performed research; G.Z., I.B., J.M.W., and B.V.L.P. contributed new reagents/analytic tools; N.I.K., I.J.B., P.F., and N.K. analyzed data; and N.I.K., R.H., H.W., and N.K. wrote the paper.

The authors declare no conflict of interest.

This article is a PNAS Direct Submission.

Freely available online through the PNAS open access option.

[1]To whom correspondence may be addressed. Email: naoto.kawakami@med.uni-muenchen.de or hwekerle@neuro.mpg.de.

This article contains supporting information online at www.pnas.org/lookup/suppl/doi:10.1073/pnas.1701806114/-/DCSupplemental.

elements in the autoimmune pathogenesis of EAE and multiple sclerosis (MS), our study opens avenues for therapy.

Results

Calcium Activity of Activated T Cells in Autoantigen-Free Peripheral Lymphatic Organs. Ex vivo activated, i.v.-infused encephalitogenic effector T cells travel through the lung vasculature before arriving in the peripheral lymphatic organs, first in the lung-draining perithymic lymph nodes and then in the spleen. The T cells settle in the splenic paracortical milieu, where they perambulate apparently at random, making brief contacts with local stroma cells (5, 16). During their sojourn, in the absence of specific autoantigens, the T cells radically rearrange their gene expression profile, acquiring a specialized phenotype that facilitates their passage through the BBB (5, 6). The nature of the signals that initiate and drive this differentiation has remained open so far.

To document signal-dependent calcium responses, we transferred in vitro-activated, MBP-specific T cells transduced to express a genetic calcium indicator ($T_{MBP\text{-}Twitch1}$ cells) i.v. into naive recipient animals. The cells first accumulated in the lung, then in lymph nodes and spleen, where they started a random walk through the paracortical areas. Importantly, at the time of transfer, the autoimmune T cells showed only very little calcium activity. However, once arrived in the spleen, the $T_{MBP\text{-}Twitch1}$ cells started off with sporadically firing brief calcium signals (Fig. 1 *A*–*C* and Movies S1 and S2). These calcium signals were defined by setting the threshold to a FRET level ($\Delta R/R \geq 1.282$), which was above the maximal level reached spontaneously by 95% of $T_{MBP\text{-}Twitch1}$ cells in the spleen. Most of the calcium signaling was short-lived (shorter than 2 min), and commonly it was associated with lowered motility (Fig. 1*C*). Control $T_{OVA\text{-}Twitch1}$ cells behaved like autoimmune $T_{MBP\text{-}Twitch1}$ cells (Fig. 1*A* and Movies S1 and S3). Anti-MHC class II-blocking antibody minimally reduced the frequency of calcium signaling, thus arguing against classic antigen recognition (Fig. 1*D*). Both $T_{MBP\text{-}Twitch1}$ and $T_{OVA\text{-}Twitch1}$ cells were also imaged in the lung, where encephalitogenic T cells first accumulate

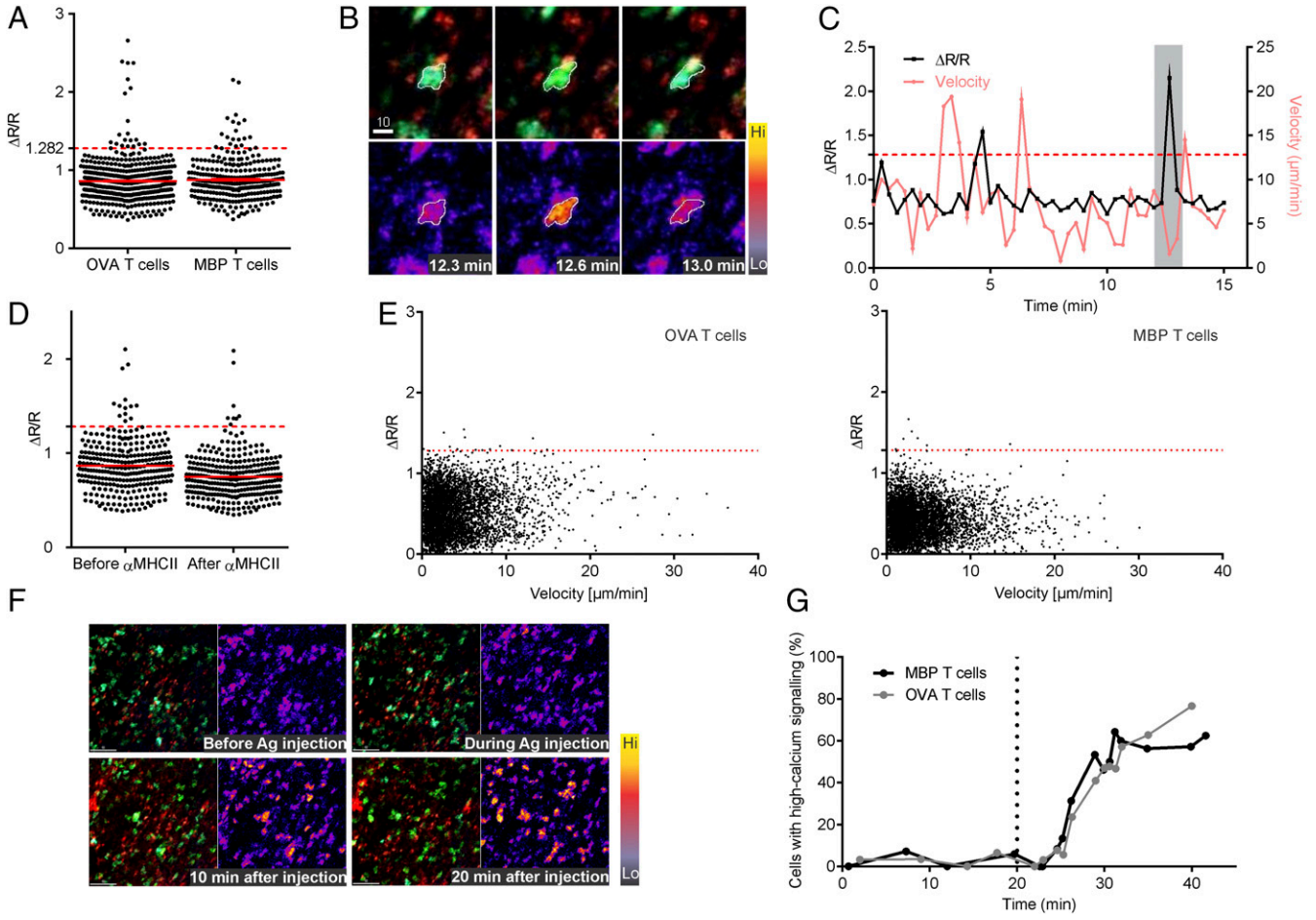

Fig. 1. Calcium signaling in the spleen. (*A*) Twitch1-labeled T cells were imaged in the spleen on day 3 p.t. Cumulative plots of the calcium level (ΔR/R) are shown. Each dot represents a single time point in a particular cell. Hereafter, dotted horizontal lines (red) indicate the threshold (1.282) of the calcium level. Representative data from two independent experiments per cell line are shown. (*B*) Series from in vivo calcium imaging of the spleen with $T_{OVA\text{-}Twitch1}$ cells. A fluorescence overlay of $T_{OVA\text{-}Twitch1}$ cells encircled (*Left*) and a pseudocolor ratio image with T cells encircled (*Right*) are depicted. The inserted numbers indicate the relative time after the start of image acquisition. (Scale bar: 10 μm.) (*C*) Representative track for intracellular calcium levels (black line) and T-cell velocities (red line) in the spleen with two episodes of short high-calcium signalings. The gray area indicates the three imaging frames from *B*. (*D*) Cumulative plots of the calcium level (ΔR/R) before and after MHC class II treatment are shown. Each dot represents a single time point in a particular cell. (*E*) Scatterplots showing $T_{OVA\text{-}Twitch1}$ or $T_{MBP\text{-}Twitch1}$ velocity versus calcium-indicator ratio change for day 1 and day 2 p.t. in the lung. Cumulative results from four independent experiments are shown. (*F*) Soluble antigen treatment. Series from in vivo calcium imaging of the spleen with $T_{OVA\text{-}Twitch1}$ cells before and after soluble antigen treatment are shown. A fluorescence overlay of $T_{OVA\text{-}Twitch1}$ cells (*Left*) and a pseudocolor ratio image with T cells (*Right*) are depicted. (Scale bar: 50 μm.) T cells (blue/yellow) and phagocytes (red, visualized by detecting autofluorescence and i.v. infusion of fluorescent dextran) are shown in fluorescent overlay. (*G*) Time kinetics for the proportion of $T_{MBP\text{-}Twitch1}$ (black line) and $T_{OVA\text{-}Twitch1}$ (gray line) cells with high-calcium levels. The vertical line indicates the time point of soluble antigen treatment. The results are representative of at least three independent experiments.

and initiate their licensing process (6). Calcium signaling in both types of lung resident T cells was extremely low, even lower than seen in the spleen (Fig. 1*E*).

Supply of soluble antigen radically changed the behavior of intrasplenic T cells. Within minutes after the infusion of MBP or OVA, most cognate T cells clustered around APCs (16), emitting long-lasting high-calcium signals (Fig. 1 *F* and *G*) (Movies S2 and S3, second half). $T_{MBP\text{-}Twitch1}$ cells and $T_{OVA\text{-}Twitch1}$ cells responded with similar time kinetics (Fig. 1*G*). Thus, in antigen-free milieus, T cells display sparse calcium signals, which in the spleen are exclusively short-lasting.

Calcium Responses Around the Blood–Brain Barrier. Having reached full migratory competence, encephalitogenic $T_{MBP\text{-}Twitch1}$ cells leave the 2° lymphoid organs for the leptomeningeal blood vessels enveloping the spinal cord. Upon arrival, the T cells first roll and then crawl along the intraluminal vascular surface (7). Our setup of two-photon microscopy detected individual rolling T cells as a series of rounded cells within one single time frame (Fig. 2*A* and Fig. S1). While rolling along the luminal surface, the T cells displayed no detectable calcium activity. In fact, their calcium levels were mostly below the threshold (Fig. 2*B*). Calcium activity was also largely absent throughout subsequent crawling, regardless of the antigen specificity and individual velocity (Fig. 2*C*). As previously reported (8), a NFAT-based sensor was not translocated to the nucleus, thus confirming that during the intraluminal phase, the T cells remain nonactivated.

The earliest $T_{MBP\text{-}Twitch1}$ cells, which pass through the vascular wall into the leptomeningeal space [prodromal day 2 post transfer (p.t.)] encounter a naive, resting milieu. There, they scan the perivascular areas, searching for APCs to make contacts of variable duration (Fig. 3*A* and Fig. S2 *A–C*, and Movie S4). We found that some, but not all of the T-cell–APC encounters were followed by intracellular high-calcium signals that ranged from scattered, short-lived peaks to sustained high plateaus (Fig. 3 and Fig. S2*G*).

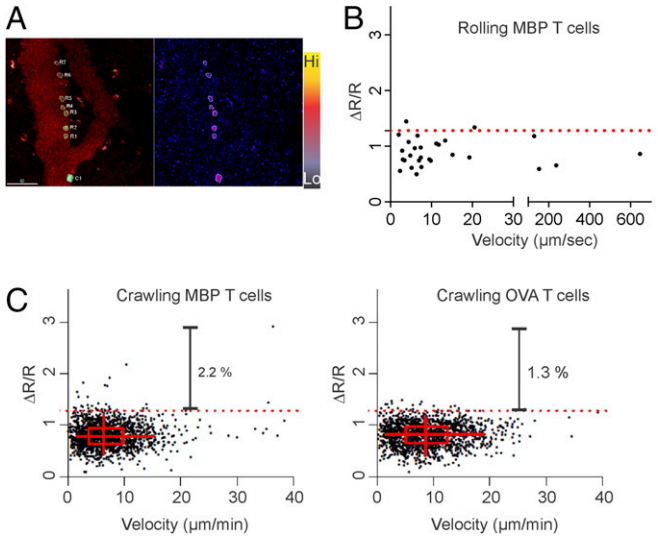

Fig. 2. Activation statuses of intraluminal T cells. (*A*) Z projection of images (Fig. S1) reveals a trace of a rolling cell (R1–R7) and a crawling cell (C1). (Scale bar: 50 μm.) A fluorescence overlay of $T_{MBP\text{-}Twitch1}$ cells (*Left*) and a pseudocolor ratio image with T cells (*Right*) are depicted. T cells (blue/yellow) and blood vessels (red, visualized by i.v. infusion of fluorescent dextran) are shown in fluorescent overlay. (*B*) Scatterplot showing $T_{MBP\text{-}Twitch1}$ velocity versus calcium-indicator ratio change for each individual time point during rolling. The results are the sum of at least three independent experiments. (*C*) Scatterplots showing $T_{MBP\text{-}Twitch1}$ and $T_{OVA\text{-}Twitch1}$ velocity versus calcium-indicator ratio change for each individual time point during crawling. $T_{MBP\text{-}Twitch1}$ (2.2%) and $T_{OVA\text{-}Twitch1}$ (1.3%) rarely showed calcium signaling. The results are the sum of at least three independent experiments.

These reactions led to T-cell activation, as previously documented by the NFAT–GFP sensor (8). Similar to EAE in the mouse (12), the velocity of the T cells was inversely correlated to shape and amplitude of calcium signaling (Fig. 3*B*).

The behavior of $T_{MBP\text{-}Twitch1}$ cells changed on day 3 p.t., at the onset of clinical EAE. At this time, the local milieu was dominated by inflammation, allowing a mass influx of effector T cells through the BBB and penetration into the parenchyma. At this stage, the immigrant effector T cells scanned the entire leptomeningeal space (Fig. S2 *D–F*) with correspondingly extensive calcium responses. The responses resembled those on day 2 p.t., with similar rates of elevated calcium signals (Fig. 3 *C* and *D* and Movie S5). However, unexpectedly, the duration of high-calcium signaling was reduced. On day 3 p.t., elevated and sustained intracellular calcium signaling lasted less than 20 min (Fig. 3*E* and Fig. S2*G*), whereas in the earlier intruders (day 2 p.t.), responses took more than 1 h. These sustained calcium signals in T cells lend strong support to the critical role of leptomeningeal interactions in the pathogenesis of CNS inflammation.

Antigen Presentation in the Leptomeninges. Several arguments suggest that the strong calcium responses by T cells in the leptomeningeal space and parenchyma reflect the recognition of locally presented autoantigen. First, OVA-specific T cells, which do not spontaneously infiltrate the CNS, can be directed there following the intrathecal instillation of OVA-presenting APCs (7). Also, OVA-specific T cells are escorted into the CNS by cotransferred MBP-specific T cells. Both conditions open the BBB and create an inflammatory microenvironment (5). As reported before (7, 17), and also in our present study, escorted $T_{OVA\text{-}Twitch1}$ cells moved much faster through the spinal cord leptomeninges than $T_{MBP\text{-}Twitch1}$ cells and did not cluster around APCs (Fig. 4 *A* and *B*). Furthermore, the infiltrating $T_{OVA\text{-}Twitch1}$ cells only sporadically emitted calcium signaling (Fig. 4*A*, Fig. S3, and Movie S6), less than once per hour (Fig. 4*C*). Less than 1% of the analyzed $T_{OVA\text{-}Twitch1}$ cells tracked showed high-calcium signals, and these were short-lived (Fig. 4*D*). In contrast, the $T_{MBP\text{-}Twitch1}$ cells spiked 8.6 times per hour on average (Fig. 4*C*), with calcium signaling of both long and short duration (Fig. 4*D*).

Furthermore, anti-MHC class II MAbs increased the motility of autoimmune $T_{MBP\text{-}Twitch1}$ cells to the level of control $T_{OVA\text{-}Twitch1}$ cells (Fig. 4 *A* and *B* and Movie S7). At the same time, the treatment reduced the number of calcium signaling in $T_{MBP\text{-}Twitch1}$ cells to less than once per hour, again similar to $T_{OVA\text{-}Twitch1}$ cells (Fig. 4 *C* and *D* and Fig. S3), whereas irrelevant anti-MHC class I MAbs affected neither locomotion nor calcium responses (Fig. 4 *A–D* and Movie S8). Anti-MHC class II blockade operated over extensive areas along the spinal cord, as shown by panoramic pictures (Fig. 4*E*), and significantly ameliorated clinical EAE (Fig. S4). Moreover, i.v. injection of this antibody did not affect established EAE, pointing to T-cell (re)activation in the CNS as a prerequisite of clinical EAE (Fig. S4). Thus, MHC-dependent antigen presentation in the CNS leptomeninges controls CNS inflammation.

In addition, we applied the nicotinic acid adenine dinucleotide phosphate (NAADP)-antagonist, BZ194, which is known to block the intracellular calcium signaling in vivo and to ameliorate clinical EAE (18). As shown in Fig. 5, BZ194 efficiently reduced intracellular calcium signaling in the T cells at leptomeninges. This reduction was mainly due to suppression of long-lasting calcium signaling, whereas short-lasting calcium signaling remains after BZ194 treatment (Fig. 5*C*). Taken together with the observation that BZ194 treatment ameliorates clinical EAE (18), the results suggest that blocking calcium signaling in T cells at this stage can be used as a therapeutic target.

Leptomeningeal APCs with Disparate Functional Potential. Quite commonly CNS-infiltrating T cells visited certain APCs without being arrested and activated. To learn whether this variant

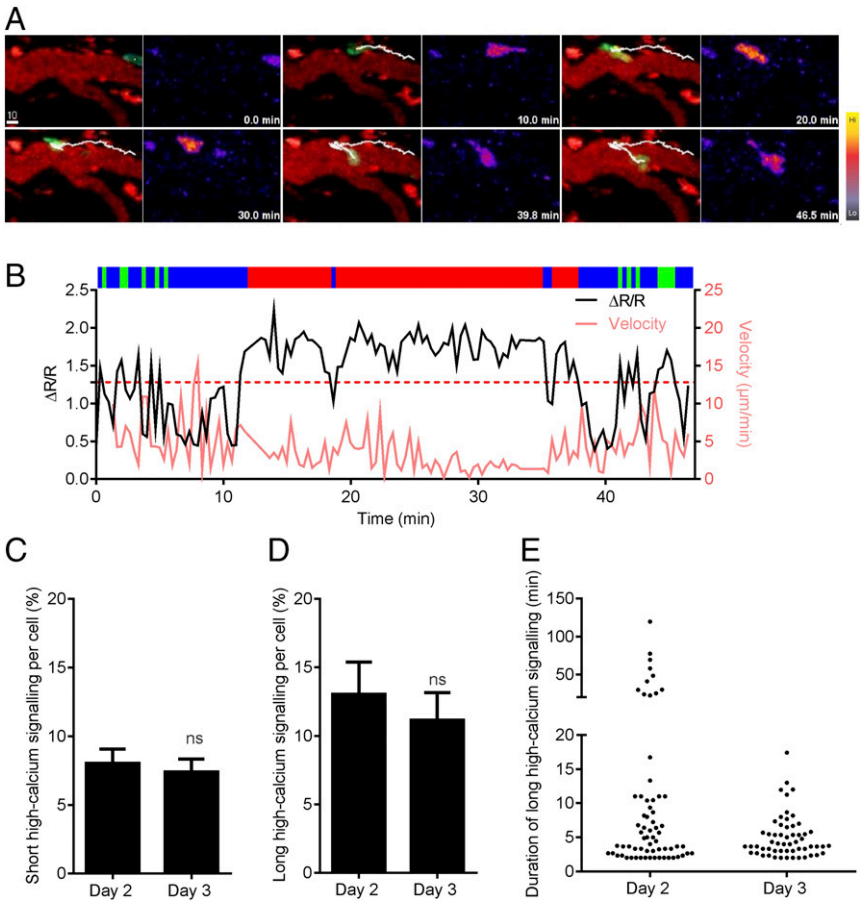

Fig. 3. T-cell activation at different stages of EAE. (*A*) A series from in vivo calcium imaging of the meninges on day 2 p.t. is depicted. A fluorescence overlay of $T_{MBP\text{-}Twitch1}$ cells (*Left*) and a pseudocolor ratio image (*Right*) are shown. A trajectory line (white) is overlaid and represents a single $T_{MBP\text{-}Twitch1}$ cell track. The inserted numbers indicate the relative time after the start of image acquisition. (Scale bar: 10 μm.) T cells (blue/yellow), blood vessels (red, visualized by i.v. infusion of fluorescent dextran), and phagocytes (red, visualized by intrathecally injected fluorescent dextran) are shown in fluorescent overlay. (*B*) Representative track of a $T_{MBP\text{-}Twitch1}$ cell (depicted in *A*) showing the intracellular calcium levels (black line) and T-cell velocities (red line) in the meninges on day 2 p.t. The dotted line depicts the ΔR/R threshold. A calcium history plot is overlaid. A blue color indicates low calcium levels, a green color indicates high calcium levels shorter than 2 min, and a red color indicated high calcium levels longer than 2 min. (*C* and *D*) The percentage of short (<2 min, *C*) or long (>2 min, *D*) high-calcium signaling per track on days 2 and 3. (*E*) Cumulative plots of long high-calcium signaling (over 2 min) on days 2 and 3. (*C* and *D*) Two-tailed *t* test is applied for statistical evaluation. (*C*–*E*) The results are the sum of at least three independent experiments.

behavior reflected a deficient antigen-presenting capacity of these individual APCs, we identified all visible APCs in the imaging area and evaluated their stimulatory capacity by calculating the percentage of T cells activated after contact (Fig. 6, Fig. S5, and Movie S9). For example, APC no. 12 in Fig. 6*A* had a strong potential to stimulate T cells, whereas other APCs, such as APC no. 3, hardly induced any T-cell activation, although several T cells passed by (Fig. S5). The potential of each APC (the time proportion of high-calcium signaling during a contact) was calculated and presented in Fig. 6*B*. The different stimulatory potential of each APC is supported by the calcium history of T cells, which are activated by contacts with a subset of APCs (Fig. 6*C*). Thus, the potential of activating encephalitogenic T cells seems to reflect an inherent property of individual APCs, rather than the variable efficiency of intracellular contacts.

Antigen Presentation in the Spinal Cord Parenchyma. The optic penetration of two-photon microscopy into myelinated tissue is limited and thus insufficient to screen the entire spinal cord parenchyma (19). We therefore studied T cellular calcium responses ex vivo using acute spinal cord explants. As described before (17), most of the infiltrating $T_{MBP\text{-}Twitch1}$ cells moved freely throughout the packed myelinated white matter, whereas some were arrested around local cells. As in the leptomeninges, the immobilized T cells responded with elevated intracellular calcium levels (Fig. 7*A*). To identify the interaction partners of $T_{MBP\text{-}Twitch1}$ cells, we focused on the two potential APC species, microglia and macrophages. We impregnated spinal cord slices with fluorescent isolectin B4, which tags microglia as well as infiltrating monocytes/macrophages. Two-photon imaging confirmed functional interaction between $T_{MBP\text{-}Twitch1}$ cells and local phagocytes (Fig. 7*A*). The arrested $T_{MBP\text{-}Twitch1}$ cells showed both short- and long-lived calcium responses. We examined full T-cell activation in the CNS parenchyma quantifying the nuclear translocation of NFAT–GFP sensors in fixed tissue sections. As expected, MBP-specific T cells were fully reactivated both in the spinal cord meninges and in the parenchyma (Fig. 7*B*), but nature and origin (resident or infiltrate derived) of the parenchymal APCs remain to be determined.

Discussion

Most T lymphocytes are migratory cells. They are not confined to one particular tissue but circulate through diverse microenvironments, where they receive signals that control their state of activation, determine their function, and guide them to their next destination. Much of this exogenous information is translated into intracellular calcium oscillations, which, depending on their frequency, duration, and topography, are integrated by decoding

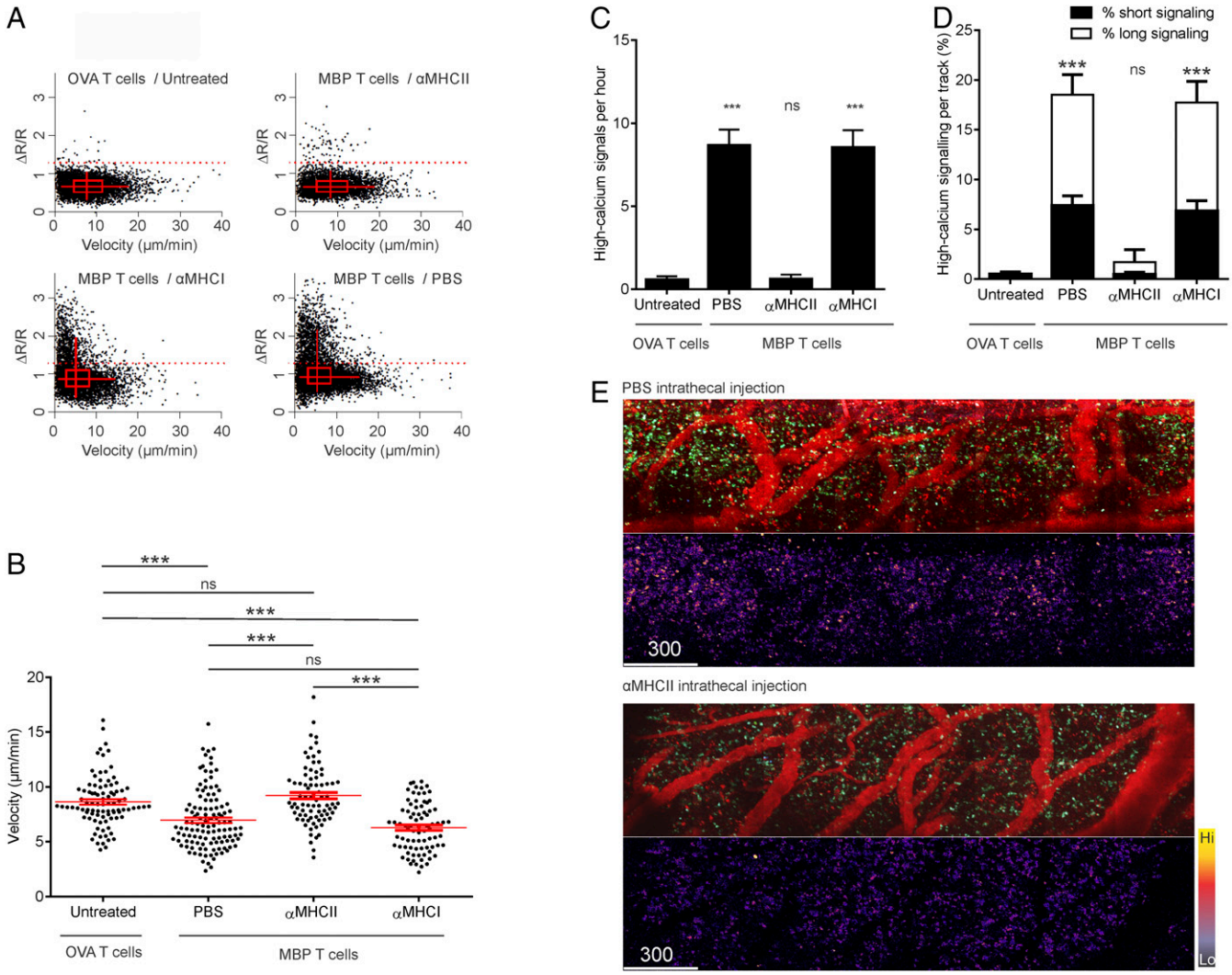

Fig. 4. Activation statuses of T cells within the spinal cord leptomeninges. (*A*) Scatterplots showing $T_{OVA\text{-}Twitch1}$ or $T_{MBP\text{-}Twitch1}$ velocity versus calcium-indicator ratio change for each individual time point with or without antibody treatment. Mean values for ΔR/R and velocity are indicated along with a 2D box plot. (*B*) Quantification of the average T-cell velocity in the spinal cord leptomeninges with or without antibody treatment. (*C*) Frequency of high-calcium signals over the threshold normalized per hour and (*D*) the proportion of short or long high-calcium signaling during imaging are shown. (*A–D*) The results are the sum of at least three independent experiments per treatment. (*E*) Representative panoramic pictures of $T_{MBP\text{-}Twitch1}$ cells (blue/yellow) in the spinal cord leptomeninges after PBS or αMHCII intrathecal injection are shown. Blood vessels (red) were visualized by i.v. infusion of fluorescent dextran. Fluorescence overlay (*Upper*) and a pseudocolor ratio image (*Lower*) were obtained from intravital imaging on day 3 p.t. (Scale bar: 300 μm.) (*B–D*) One-way ANOVA is applied for statistical evaluation.

proteins to determine the characteristics of a transcriptional response (20). A prominent player in the decoding of immune signals is NFAT, a transcription factor, which, in an inactive state, locates in the cytoplasm, but following high-calcium signaling, translocates into the nucleus.

A highly suitable model to illustrate the variable fate of immune cells is T-cell–transferred EAE in the Lewis rat. This variant of EAE model allows tracing freshly activated encephalitogenic T cells as they travel through several distinct cellular milieus, where they successively interact with local cells in the presence or absence of cognate antigen, before they ultimately enter their final destination, the CNS white matter (5). Importantly, in this system, T-cell infiltration into the CNS follows a highly reproducible time kinetic that allows detection of calcium signaling in T cells at different migration steps. In an attempt to decipher the signaling steps that occur in sequential milieus of living animals, we have recently developed two genetic indicators, one displaying calcium signals by FRET imaging, and the other indicating subsequent NFAT activation. As a calcium indicator, we now applied an improved version of the previously described indicator Twitch1 (12) engineered to optimize its expression in rat T cells. As key modifications, the retroviral payload was reduced to 1.3 kb by shifting the neomycin resistance gene outside of the long terminal repeats (LTRs), which maintains the antibiotic selection of the packaging cells (Fig. S6) (21). Importantly, while emitting strong recordable signals, the indicator system did not interfere with the encephalitogenic function (Fig. S7). This indicator allows the documentation of changes in the intracellular calcium levels, although the limited scanning speed of our intravital two-photon setup (~1 s per frame) does not resolve calcium oscillations of <1 Hz. Elevated and sustained calcium signaling may induce NFAT translocation from the cytosol to the nucleus, a process that we followed using a recently described NFAT–GFP fusion protein (8).

Fully activated myelin-specific T cells do not directly enter the CNS parenchyma; they first have to spend time in the periphery (22), where they become licensed for CNS invasion (5, 6). The first milieus visited by T-cell blasts after i.v. transfer are located in the peripheral organs, in particular in the 2° lymphatic tissues,

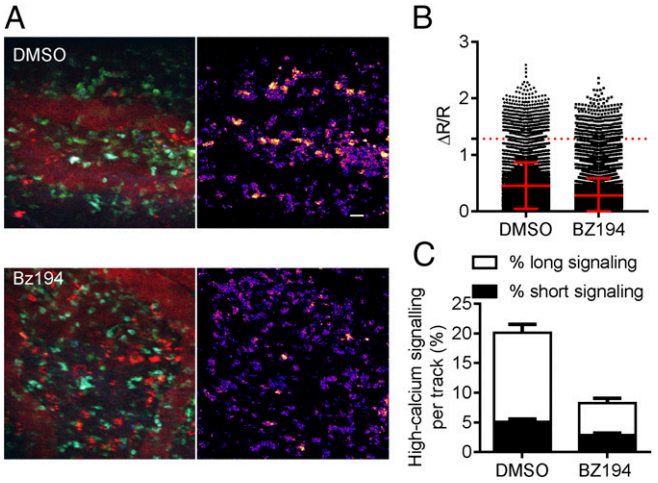

Fig. 5. Effect of BZ194 on calcium signaling in T cells. (*A*) Representative pictures of $T_{MBP\text{-}Twitch1}$ cells (blue/yellow) in the spinal cord leptomeninges after BZ194 or control (DMSO) treatment on day 3 p.t. Blood vessels (red) were visualized by i.v. infusion of fluorescent dextran. (Scale bar: 20 μm.) (*B*) Cumulative plots of the calcium level (ΔR/R) are shown. Each dot represents a single time point in a particular cell. (*C*) Frequency of short (<2 min) and long (>2 min) high-calcium signaling were analyzed. Representative (*A*) or cumulative (*B* and *C*) results from three independent experiments.

including the spleen and lung. There, the effector T cells are reprogrammed to pass through the BBB, mostly within the leptomeninges. This maturation process involves the down-regulation of activation markers but at the same time the induction of gene products facilitating locomotion and cellular homing (6). Reeducation takes place in the paracortical areas of 2° lymphatic tissues, which are occupied by T cells, dendritic cells (DCs), macrophages, and fibroblastic reticular cells (23). The newly arrived effector cells continually meander through the packed tissue apparently at random, forming very few stable contacts with the surrounding stroma cells. Nevertheless, the rambling cells show characteristic brief calcium signaling events (Fig. 1), which, however, do not lead to NFAT translocation (Fig. 7*B*). This behavior occurs in the absence of specific antigen and is blocked partially by anti-MHC class II antibodies. In contrast, infusion of soluble antigen results in the immediate arrest of specific T cells around the APCs and the sustained elevation of intracellular calcium levels. In line with our present observation, antigen-independent intracellular calcium signaling was noted previously in vitro, with naive $CD4^+$ T cells producing calcium signaling upon interactions with DCs (24). These antigen-independent calcium signals were weaker and shorter than those produced by T-cell receptor (TCR)/antigen-mediated signals but they seemed to depend on the formation of immunological synapses. This reprogramming of effector T cells seems to be initiated in the lung (6), with remarkably low calcium activity, arguing against a major role of calcium signaling in this particular stage of T-cell licensing.

Continuous signaling via the TCR seems to provide tonic signals to support the function and survival of T cells in general (25) and of Treg cells in particular (26, 27). It should be noted that our system exclusively involves autoimmune effectors, with no evidence of Treg cells (Fig. S7*C*). GPCRs responding to chemokine signals are known to act via calcium changes, which in

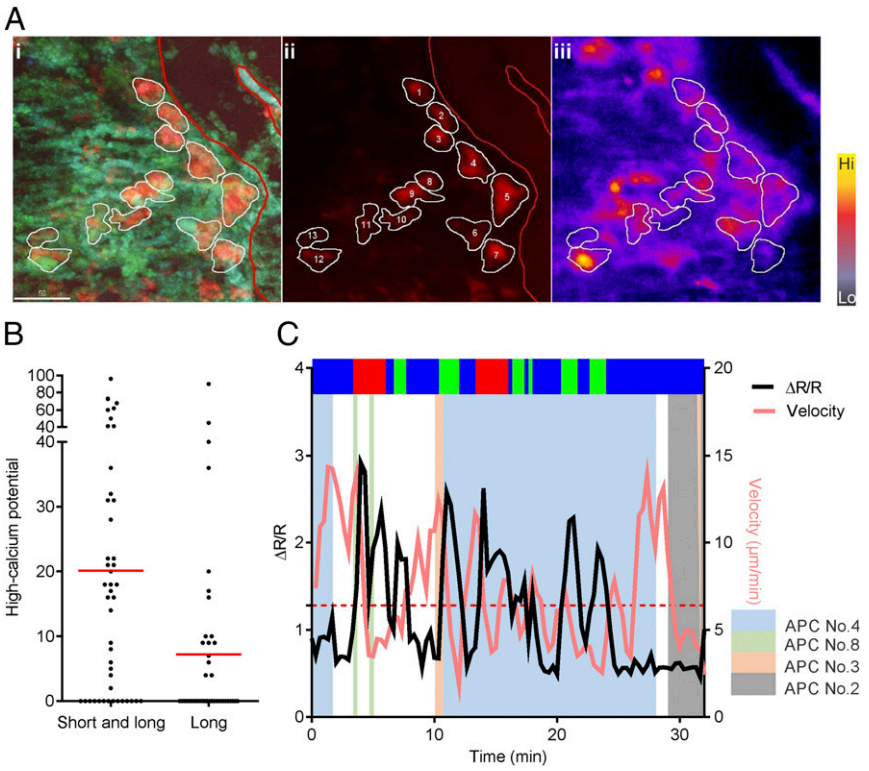

Fig. 6. Verifying APC potential in the spinal cord leptomeninges. (*A*) Sample images from in vivo calcium imaging of leptomeningeal vessels on day 3 p.t. A fluorescence overlay of $T_{MBP\text{-}Twitch1}$ cells and APCs which are visualized by intrathecally injected fluorescent dextran (*i*), only APCs (*ii*), and a pseudocolor ratio image with $T_{MBP\text{-}Twitch1}$ cells and APCs (*iii*) are depicted. APCs with high and low potential to stimulate T cells are encircled. (*B*) High-calcium potential in T cells during T-cell/APC contacts. The calcium potential depicts the time proportion of the total short and/or long high-calcium signaling during T-cell/APC contacts. Calcium potential, duration of high-calcium signaling/duration of contact × 100. The results are the sum of three independent experiments per time point. (*C*) Representative track of a $T_{MBP\text{-}Twitch1}$ cell from *A* depicting the intracellular calcium levels (black line) and T-cell velocities (red line). A series of interactions with different APCs is indicated. A calcium history plot is overlaid.

turn activate integrins to increase their affinity to specific ligands (28). Indeed, short-lasting calcium signaling in the spleen was inhibited partially by inhibitors of chemokine receptors (Fig. S8). This process may facilitate the successful passage of reprogrammed effector T cells through the BBB, which centrally involves integrins (7).

Migrant encephalitogenic T cells overcome the BBB in two phases. During the first 2 d following transfer, only small numbers of activated T cells trickle into the leptomeningeal space. Then, around day 3, there is a sharp increase, culminating in the mass invasion of millions of cells, an event that coincides with T-cell intrusion into the CNS parenchyma and the onset of neurological disease. On a single-cell level, the interaction between migrant effector T cells and the vascular BBB is stereotypic. The incoming T cell attaches to the inner vascular surface and initially rolls along, driven by the bloodstream. Then, after firm attachment, the T cell crawls on the endothelium, preferably against the bloodstream, until it passes through a gap in the vascular wall (7). Adhesion to the luminal surface critically involves integrin VLA-4, with a contribution from LFA-1. The intraluminal rolling and crawling of effector T cells proceeds without elevated calcium signaling (Fig. 2 *B* and *C*) and without translocation of NFAT (8), which is in harmony with earlier studies of cell surface markers (7). Although it is known that integrin-mediated stimulation induces intracellular calcium signaling, these signals may be too small to be detected by our Twitch reporter (12, 29).

After diapedesis, T cells roam through the leptomeningeal microenvironment apparently at random, until encountering a particular set of local phagocytes (7). These contacts involve extensive calcium spiking, with profiles varying over time. The duration of calcium signaling is longest on day 2 p.t. (Fig. 3*E*), at a time point preceding the mass invasion. This response is often observed at the perivascular area, pointing to a major contribution of perivascular macrophages in this process. Paradoxically, in this phase of CNS inflammation, the production of inflammatory cytokines is still very low (6), pointing to a limited availability of antigen/class II complexes. Indeed, this has been documented by in vitro experiments studying local APCs (7).

The stimulatory potential of individual leptomeningeal phagocytes was variable. Some APCs attracted numerous T cells and induced high-calcium responses, whereas other APCs were less active (Fig. 6). One factor contributing to this diversity may be the limited availability of immunogenic myelin proteins. In fact, we previously reported that APCs freshly isolated from naive leptomeninges present low doses of incorporated MBP to specific T cells. In addition, the infusion of myelin protein into the leptomeningeal space converted low-encephalitogenic T cells to high-encephalitogenic T cells (30).

A second factor influencing antigen presentation in the leptomeninges relates to the inflammatory status of the local milieu. The change of inflammatory status is in harmony with the hockey-stick kinetics of T-cell invasion, which proceeds gently in early phases with mostly homeostatic APCs, but explosively increases after a period of prodromal priming (7). In fact, the early invading T cells release proinflammatory factors that enable the local APCs along with infiltrating peripheral APCs to present myelin antigen to an ever-increasing number of invading T cells. Full activation, reflected both by calcium and NFAT sensors, occurred in T cells with a high pathogenic potential, but not in weakly encephalitogenic or nonencephalitogenic T cells (30). T-cell activation often started out with a series of brief contacts between T cells and APCs without NFAT–GFP displacement, but ended in sustained adhesion with nuclear NFAT translocation (8). $T_{MBP\text{-}Twitch1}$ cells also showed repeated short-lived contacts with APCs together with short-lived calcium signaling preceding arrest and long-lasting calcium signaling. This finding suggests that T cells may integrate elevated calcium signaling from multiple sources (31).

Most studies have explored calcium responses by introducing T cells loaded with small-molecular fluorochrome indicators in vivo and imaging lymph node explants (32, 33). In line with our observation (Fig. 1), they have described infrequent short-lived calcium signaling under noninflammatory conditions as well as lowered motility during the calcium spike. In addition, they have found sustained high-calcium signaling, persisting over hours, under immunized conditions, in contrast to our observation, which rarely showed contacts lasting hours with sustained calcium signaling in the spinal cord leptomeninges (Fig. 3). The difference could be explained by the quality and quantity of antigen presentation. Whereas the lymph nodes contain many professional APCs that are loaded with an excess amount of antigen provided by immunization, the quantity of local APCs in the spinal cord meninges is limited, and the APCs were not saturated by endogenous antigen, even during the acute phase of inflammation. The availability of antigen presented on APCs influences the duration of contacts and, hence, the extent of T-cell activation (34). Indeed, in the spleen, the application of an excess amount of specific antigen dramatically increased the contact duration between T cells and APCs and induced long-lasting sustained calcium signaling within T cells (Fig. 1 *F* and *G*).

We describe here the calcium fluctuations of encephalitogenic effector T cells throughout their journey after i.v. transfer into the CNS parenchyma. We distinguish two different types of calcium signaling: One was short-lived and was independent of antigen recognition. This signaling seemed to be important to reprogram fully activated T cells to the migratory phenotype required for CNS infiltration. The other calcium response was longer-lasting, depended on antigen, and arose preferentially during phases of reduced T-cell motility or during their arrest around antigen-presenting phagocytes. The sustained high-calcium signaling response results in the nuclear translocation of NFAT and in full-scale T-cell activation (8). In contrast to previous reports that showed that stable contacts with APCs induce T-cell proliferation (35), the long-lasting calcium signaling observed in the CNS is not associated with cellular proliferation, possibly due to insufficient function of CNS local APCs (7).

This work has several implications. It reveals that delivery of calcium signals from different environments is required for infiltration of encephalitogenic T cells into the CNS. Importantly, the use of activation sensors is not limited to encephalitogenic T cells, but can be adapted to other immune responses, where our approach might reveal a comparable complexity of reactions.

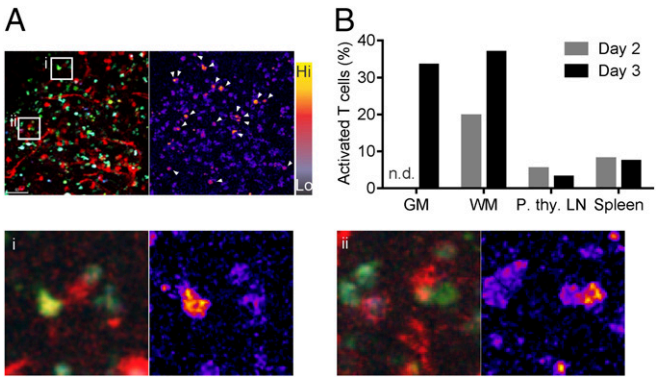

Fig. 7. Calcium signalings in encephalitogenic T cells within the spinal cord parenchyma. (*A*) Sample image from an acute explant in the parenchyma with $T_{MBP\text{-}Twitch1}$ cells. A fluorescence overlay of $T_{MBP\text{-}Twitch1}$ cells (*Left*) and a pseudocolor ratio image with T cells (*Right*) are depicted. The acute explant was stained with isolectin B4 [microglia (40), macrophages (41), and endothelial cells (42), red] and DAPI (blue) at *Left*. Cells with elevated calcium are indicated with white arrowheads. (Scale bar: 50 μm.) High-power pictures from indicated areas are shown below. (*B*) T-cell activation was detected by nuclear translocation of NFAT–GFP using PFA-fixed cryosection imaged by confocal microscopy. Results are the sum of at least two independent experiments. GM, gray matter; n.d., not detected; p. thy. LN, peri thymic lymph node; WM, white matter. GM and WM were distinguished by taking reflection images that show different structures as shown previously (7).

Finally, from a translational point of view, identification of serial checkpoints of T-cell entry may be of therapeutic interest. Indeed, blocking T-cell entry with the anti–VLA-4 monoclonal antibody natalizumab is an approved, highly effective therapy for multiple sclerosis (36, 37). Because T cells are licensed at serial checkpoints, blocking of T-cell activation is a versatile therapeutic concept for EAE/MS. Thus, the reprogramming of freshly activated T cells to a "migratory" phenotype could be one target along these lines. Indeed, the NAADP antagonist, BZ194, which efficiently blocks intracellular calcium signaling (38), ameliorates clinical EAE both by prophylactic and therapeutic application (18). In this study intravital imaging revealed that BZ194 reduced the frequency of long-lasting calcium signaling in the T cells at the spinal cord leptomeninges (Fig. 5). In addition, autoantigen presentation in the CNS compartments should be reconsidered as an early therapeutic target.

Methods

Animals. Female Lewis rats (body weight 100–150 g) were obtained from the breeding colony of the Max Planck Institute of Neurobiology. All of the animal experiments were approved by the local authority (Regierung von Oberbayern).

EAE Induction. EAE is induced by adoptive transfer of encephalitogenic T cells as described previously (7). Briefly, T cells are activated in vitro by their specific antigen presented by irradiated (50 Gy) thymus derived APCs for 2 d. The activated T cells are i.v. injected into the recipient animals. Importantly, at the time of T-cell transfer, T cells show low calcium activity.

Twitch1-Encoding Retroviral Vector. Although T cells could be efficiently transduced with pMSCV–GFP (13), replacing GFP with Twitch1 reduced the efficiency dramatically, presumably owing to the size of the construct (Fig. S6*A*, construct I). In addition, the expression of a second ORF led by a strong phosphoglycerate kinase (PGK) promoter may have decreased the expression of the Twitch1 protein, which is expressed only by the LTR promoter on the 5′ end (39).

To optimize the expression of Twitch1, we increased packaging efficiency by trimming the retrovirus to 1.3 kb, removing the neomycin resistance gene and the PGK promoter (Fig. S6*A*, construct II). To allow for selection of transfected cells, we used the PINCO vector (21), which has the neomycin resistance gene outside of the LTRs.

The reported PINCO–GFP vector (21) was digested with BspQI and blunt ends were generated using a Klenow DNA polymerase. Subsequently, the vector was further digested with SspI and EcoRI to substitute the sequence between the two LTRs with the LTRs and the *Twitch1* from the pMSCVΔneoTwitch1^{CD} vector (12). *Twitch1* including the LTRs was excised from the pMSCVΔneoTwitch1^{CD} vector by restriction digestion with SspI. This construct allows the positive selection of transfected packaging cells, which produces higher virus titers and provides higher transduction efficiency owing to its smaller RNA size (Fig. S6*A*, construct III). The resulting transduction rate was sufficient to isolate pure Twitch1-labeled T-cell populations by flow cytometry (Fig. S6*B*). The Twitch1-encoding retroviral vector was transfected into packaging cells, GP+E 86 cells (ATCC CRL-9642), using the calcium phosphate method.

Establishment of T-Cell Lines. The establishment of T-cell lines was described previously (30). Twitch1-labeled T cells were enriched by flow cytometric sorting using a MoFlow (Dako) or a FACS Aria (BD). The transduced T cells were selected by neomycin (400 μg/mL) if the vector contained a neomycin resistance gene. The expression of Twitch1 was confirmed by fluorescence microscopy using an Axiovert 200 M microscope (Zeiss Microscopy) equipped with a CoolSnap CCD camera (Roper Scientific). Importantly, the expression of Twitch1 did not alter the T-cell phenotype (Fig. S7 *A* and *B*). The effector T cells are IFNγ/IL17- or IFNγ- producing cells and do not express FoxP3 (Fig. S7*C*).

Flow Cytometric Analysis. Resting T cells were stained for the following surface markers: CD4 (W3/25), αβTCR (R73), CD25 (OX-39), CD134 (OX-40), CD49d (TA-2), CD11a (wt1), CD45RC (OX-22), CD62L (OX-85), CD11b (OX-42) (all from AbD Serotec), MHC class I (OX-18), and MHC class II (OX-6) produced in-house or with an isotype control (MOPC31c) (from Sigma). Allophycocyanin-conjugated goat anti-mouse IgG (The Jackson Laboratory) served as a secondary antibody. For FoxP3 staining, eFluor450-conjugated anti-mouse/rat FoxP3 (FJK-16s, eBioscience) were used together with Perm buffer (BD). The staining was described previously (5). All samples were measured by FACS VERSE (BD) and data analysis was performed using FlowJo software.

Intravital Imaging. Intravital imaging in the spinal cord meninges (7, 8, 12) and spleen (16), and ex vivo imaging in acute spinal cord slices, were described previously (17). Dead cells, which may have been injured during slice preparation, were excluded from the analysis using low-dose DAPI staining.

The images were processed and analyzed for intracellular calcium measurement (12). Regions of interest (ROIs) that include the outline cell shape from both T cells and APCs were automatically cross-checked in ImageJ, and any overlap or bordering of the ROIs within 0.9375 μm was considered a contact. A tolerance of one pixel was added to every ROI containing APCs. Because the dendrites of the APCs were too delicate to be visualized in detail, the interruption of a contact over one time point was considered a continuing contact.

Imaging in Explant Lung Tissue. Lungs were isolated on day 1 or day 2 after adoptive transfer of T cells. Acute slices with thickness of 300 μm were prepared by a tissue chopper. The slices were kept carbogenized in Hank's buffered salt solution (HBSS) until used for imaging. For the imaging by two-photon microscopy, the slices were stabilized with slice anchor in the dish, and superfused with carbogenized HBSS warmed to 37 °C as described previously (17).

BZ194 Treatment. BZ194 was synthesized and purified as previously described (38) and checked for homogeneity by HPLC, NMR, and high-resolution mass spectrometry. BZ194 (180 mg/kg in DMSO) was injected intraperitoneally daily starting from day 0 after EAE induction. As a control, the same volume of DMSO was given. Intravital imaging at the spinal cord leptomeninges was performed on day 3 p.t.

Retransfer After Treatment with a Chemokine Receptor Inhibitor. Twitch1-expressing T cells were prepared 3 d after adoptive transfer from the spleen (8). The lymphocytes were treated with chemokine/chemokine receptor inhibitors for 60 min before transfer to secondary recipient animals. The following inhibitors were used: PTX (List Biological Laboratories, 100 ng/mL), Maraviroc (Sigma, 25 μg/mL), AMD3100 (Sigma, 25 μg/mL), and TAK-779 (Sigma, 22 μg/mL). After treatment, 10×10^6 Twitch1-labeled T cells were washed with DMEM supplemented with 25 mM Hepes and retransferred into naive recipients via the tail vein.

Statistical Tests. For all statistical tests, we used Prism software (GraphPad) as described in the figure legends. Significance was indicated according to the *P* value as follows: $*P < 0.05$, $**P < 0.01$, $***P < 0.001$. The scatterplots were constructed using R. The overlaid box plots extend from the 25th to the 75th percentiles and the whiskers extend from the 5th to the 95th percentiles.

ACKNOWLEDGMENTS. We thank Ms. Sabine Kosin for excellent technical support and Dr. Martin Spitaler (Max Planck Institute of Biochemistry) for cell sorting. This work is supported by the Hertie Foundation (Senior Professorship to H.W.), Deutsche Forschungsgemeinschaft (DFG) (Reinhart Koselleck Project and TransRegio128), Max Planck Society and SyNergy (H.W.), DFG (TransRegio128, Research Grant KA 2651/2-1 and Heisenberg Fellowship KA2651/3-1), Novartis Foundation for Therapeutic Research, and Ludwig Maximilians University Munich (N.K.), Cyliax Stftung, "Verein Therapieforschung für Multiple Sklerose Kranke e.V." DFG (Transregio128 and SyNergy) (R.H.), and Deutscher Akademischer Austauschdienst (N.I.K.). B.V.L.P. is a Wellcome Trust Senior Investigator (Grant 101010).

1. Obermeier B, Daneman R, Ransohoff RM (2013) Development, maintenance and disruption of the blood-brain barrier. *Nat Med* 19:1584–1596.
2. Wekerle H, Sun DM (2010) Fragile privileges: Autoimmunity in brain and eye. *Acta Pharmacol Sin* 31:1141–1148.
3. Engelhardt B, Vajkoczy P, Weller RO (2017) The movers and shapers in immune privilege of the CNS. *Nat Immunol* 18:123–131.
4. Berer K, et al. (2011) Commensal microbiota and myelin autoantigen cooperate to trigger autoimmune demyelination. *Nature* 479:538–541.
5. Flügel A, et al. (2001) Migratory activity and functional changes of green fluorescent effector cells before and during experimental autoimmune encephalomyelitis. *Immunity* 14:547–560.
6. Odoardi F, et al. (2012) Encephalitogenic T cells get licensed in the lung for entry into the central nervous system. *Nature* 488:675–679.
7. Bartholomäus I, et al. (2009) Effector T cell interactions with meningeal vascular structures in nascent autoimmune CNS lesions. *Nature* 462:94–98.
8. Pesic M, et al. (2013) 2-photon imaging of phagocyte-mediated T cell activation in the CNS. *J Clin Invest* 123:1192–1201.
9. Engelhardt B, et al. (2016) Vascular, glial, and lymphatic immune gateways of the central nervous system. *Acta Neuropathol* 132:317–338.
10. Smedler E, Uhlén P (2014) Frequency decoding of calcium oscillations. *Biochim Biophys Acta* 1840:964–969.
11. Mank M, et al. (2006) A FRET-based calcium biosensor with fast signal kinetics and high fluorescence change. *Biophys J* 90:1790–1796.
12. Mues M, et al. (2013) Real-time in vivo analysis of T cell activation in the central nervous system using a genetically encoded calcium indicator. *Nat Med* 19:778–783.

13. Flügel A, Willem M, Berkowicz T, Wekerle H (1999) Gene transfer into $CD4^+$ T lymphocytes: Green fluorescent protein-engineered, encephalitogenic T cells illuminate brain autoimmune responses. *Nat Med* 5:843–847.
14. Lodygin D, et al. (2013) A combination of fluorescent NFAT and H2B sensors uncovers dynamics of T cell activation in real time during CNS autoimmunity. *Nat Med* 19: 784–790.
15. Marangoni F, et al. (2013) The transcription factor NFAT exhibits signal memory during serial T cell interactions with antigen-presenting cells. *Immunity* 38:237–249.
16. Odoardi F, et al. (2007) Instant effect of soluble antigen on effector T cells in peripheral immune organs during immunotherapy of autoimmune encephalomyelitis. *Proc Natl Acad Sci USA* 104:920–925.
17. Kawakami N, et al. (2005) Live imaging of effector cell trafficking and autoantigen recognition within the unfolding autoimmune encephalomyelitis lesion. *J Exp Med* 201:1805–1814.
18. Cordiglieri C, et al. (2010) Nicotinic acid adenine dinucleotide phosphate-mediated calcium signalling in effector T cells regulates autoimmunity of the central nervous system. *Brain* 133:1930–1943.
19. Romanelli E, et al. (2013) Cellular, subcellular and functional in vivo labeling of the spinal cord using vital dyes. *Nat Protoc* 8:481–490.
20. Dolmetsch RE, Xu K, Lewis RS (1998) Calcium oscillations increase the efficiency and specificity of gene expression. *Nature* 392:933–936.
21. Grignani F, et al. (1998) High-efficiency gene transfer and selection of human hematopoietic progenitor cells with a hybrid EBV/retroviral vector expressing the green fluorescence protein. *Cancer Res* 58:14–19.
22. Wekerle H, Linington C, Lassmann H, Meyermann R (1986) Cellular immune reactivity within the CNS. *Trends Neurosci* 9:271–277.
23. Turley SJ, Fletcher AL, Elpek KG (2010) The stromal and haematopoietic antigen-presenting cells that reside in secondary lymphoid organs. *Nat Rev Immunol* 10: 813–825.
24. Revy P, Sospedra M, Barbour B, Trautmann A (2001) Functional antigen-independent synapses formed between T cells and dendritic cells. *Nat Immunol* 2:925–931.
25. Hochweller K, et al. (2010) Dendritic cells control T cell tonic signaling required for responsiveness to foreign antigen. *Proc Natl Acad Sci USA* 107:5931–5936.
26. Levine AG, Arvey A, Jin W, Rudensky AY (2014) Continuous requirement for the TCR in regulatory T cell function. *Nat Immunol* 15:1070–1078.
27. Vahl JC, et al. (2014) Continuous T cell receptor signals maintain a functional regulatory T cell pool. *Immunity* 41:722–736.
28. Dixit N, Simon SI (2012) Chemokines, selectins and intracellular calcium flux: Temporal and spatial cues for leukocyte arrest. *Front Immunol* 3:188.
29. Weismann M, et al. (1997) Integrin-mediated intracellular Ca^{2+} signaling in Jurkat T lymphocytes. *J Immunol* 158:1618–1627.
30. Kawakami N, et al. (2004) The activation status of neuroantigen-specific T cells in the target organ determines the clinical outcome of autoimmune encephalomyelitis. *J Exp Med* 199:185–197.
31. Henrickson SE, et al. (2008) T cell sensing of antigen dose governs interactive behavior with dendritic cells and sets a threshold for T cell activation. *Nat Immunol* 9:282–291.
32. Matheu MP, et al. (2008) Imaging of effector memory T cells during a delayed-type hypersensitivity reaction and suppression by Kv1.3 channel block. *Immunity* 29: 602–614.
33. Wei SH, et al. (2007) Ca^{2+} signals in $CD4^+$ T cells during early contacts with antigen-bearing dendritic cells in lymph node. *J Immunol* 179:1586–1594.
34. Celli S, Lemaître F, Bousso P (2007) Real-time manipulation of T cell-dendritic cell interactions in vivo reveals the importance of prolonged contacts for $CD4^+$ T cell activation. *Immunity* 27:625–634.
35. Mempel TR, Henrickson SE, Von Andrian UH (2004) T-cell priming by dendritic cells in lymph nodes occurs in three distinct phases. *Nature* 427:154–159.
36. Yednock TA, et al. (1992) Prevention of experimental autoimmune encephalomyelitis by antibodies against α 4 β 1 integrin. *Nature* 356:63–66.
37. Steinman L (2012) The discovery of natalizumab, a potent therapeutic for multiple sclerosis. *J Cell Biol* 199:413–416.
38. Dammermann W, et al. (2009) NAADP-mediated Ca^{2+} signaling via type 1 ryanodine receptor in T cells revealed by a synthetic NAADP antagonist. *Proc Natl Acad Sci USA* 106:10678–10683.
39. Cepko C, Pear W (2001) Overview of the retrovirus transduction system. *Curr Protoc Mol Biol* 9:Unit9.9.
40. Pennell NA, Hurley SD, Streit WJ (1994) Lectin staining of sheep microglia. *Histochemistry* 102:483–486.
41. Maddox DE, Shibata S, Goldstein IJ (1982) Stimulated macrophages express a new glycoprotein receptor reactive with Griffonia simplicifolia I-B4 isolectin. *Proc Natl Acad Sci USA* 79:166–170.
42. Laitinen L (1987) Griffonia simplicifolia lectins bind specifically to endothelial cells and some epithelial cells in mouse tissues. *Histochem J* 19:225–234.

Supporting Information

Kyratsous et al. 10.1073/pnas.1701806114

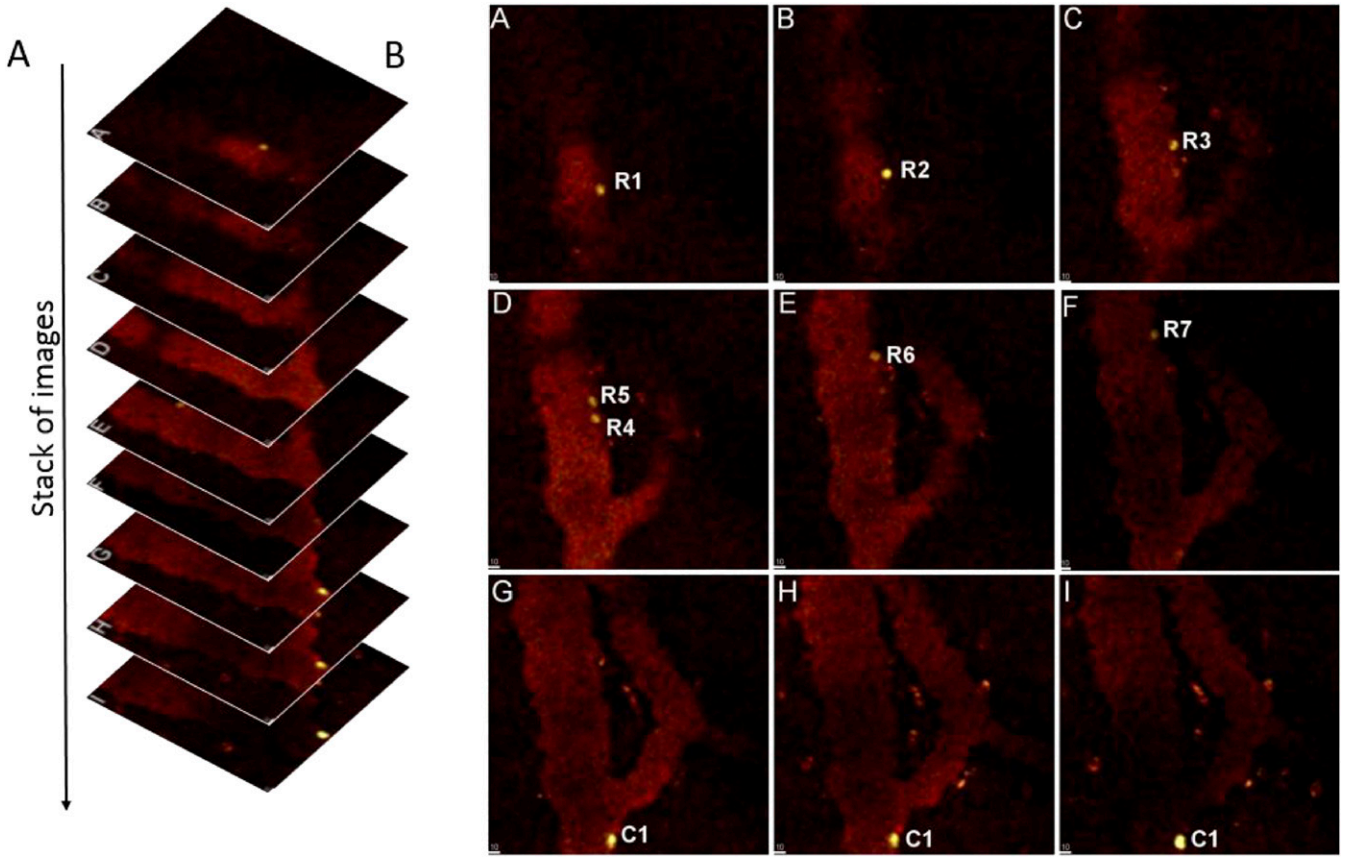

Fig. S1. Detection of rolling and crawling cells by two-photon microscopy. Scheme to detect rolling and crawling cells. (*A*) Scanning of z dimension acquires a series of images. (*B*) Typical cellular size is 10 μm. Because the z interval is around 3–4 μm, one cell can be detected multiple times. The motility of rolling T cells is very high; therefore, a rolling cell locates at different *x*–*y* position in subsequent frames because acquisition of a *x*–*y* plane needs ∼1 s in our setup. For example, a rolling cell appears in six z planes (*A*–*F*) in different positions (R1–R7). In images *G*–*I*, a crawling cell appears (C1). T cells (blue/yellow) and blood vessels (red, visualized by i.v. infusion of fluorescent dextran) are shown in fluorescent overlay. (Scale bar: 10 μm.)

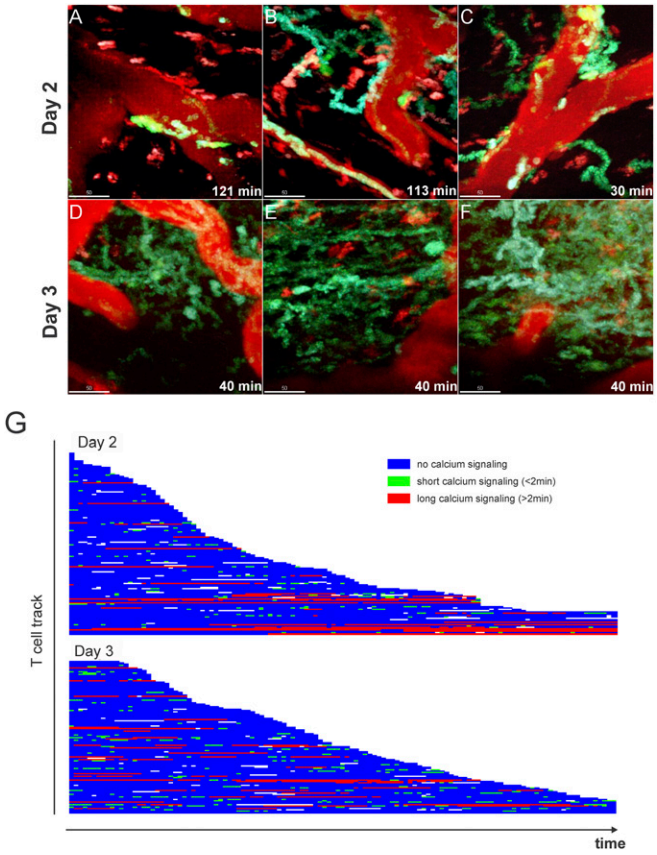

Fig. S2. Leptomeningeal scanning of encephalitogenic T cells on day 2 and day 3. Time projections from six representative movies are shown for $T_{MBP\text{-}Twitch1}$ cells (green) and blood vessels (red, visualized by i.v. infusion of fluorescent dextran) on day 2 (*A*–*C*) and day 3 p.t. (*D*–*F*). Inserted numbers indicate the duration of image acquisition. (*G*) Calcium history plots of $T_{MBP\text{-}Twitch1}$ cells on days 2 and 3 p.t. Each horizontal line represents a single T-cell track. In the calcium history plots, a blue color indicates low calcium levels, a green color indicates high calcium levels shorter than 2 min, and a red color indicated high calcium levels longer than 2 min.

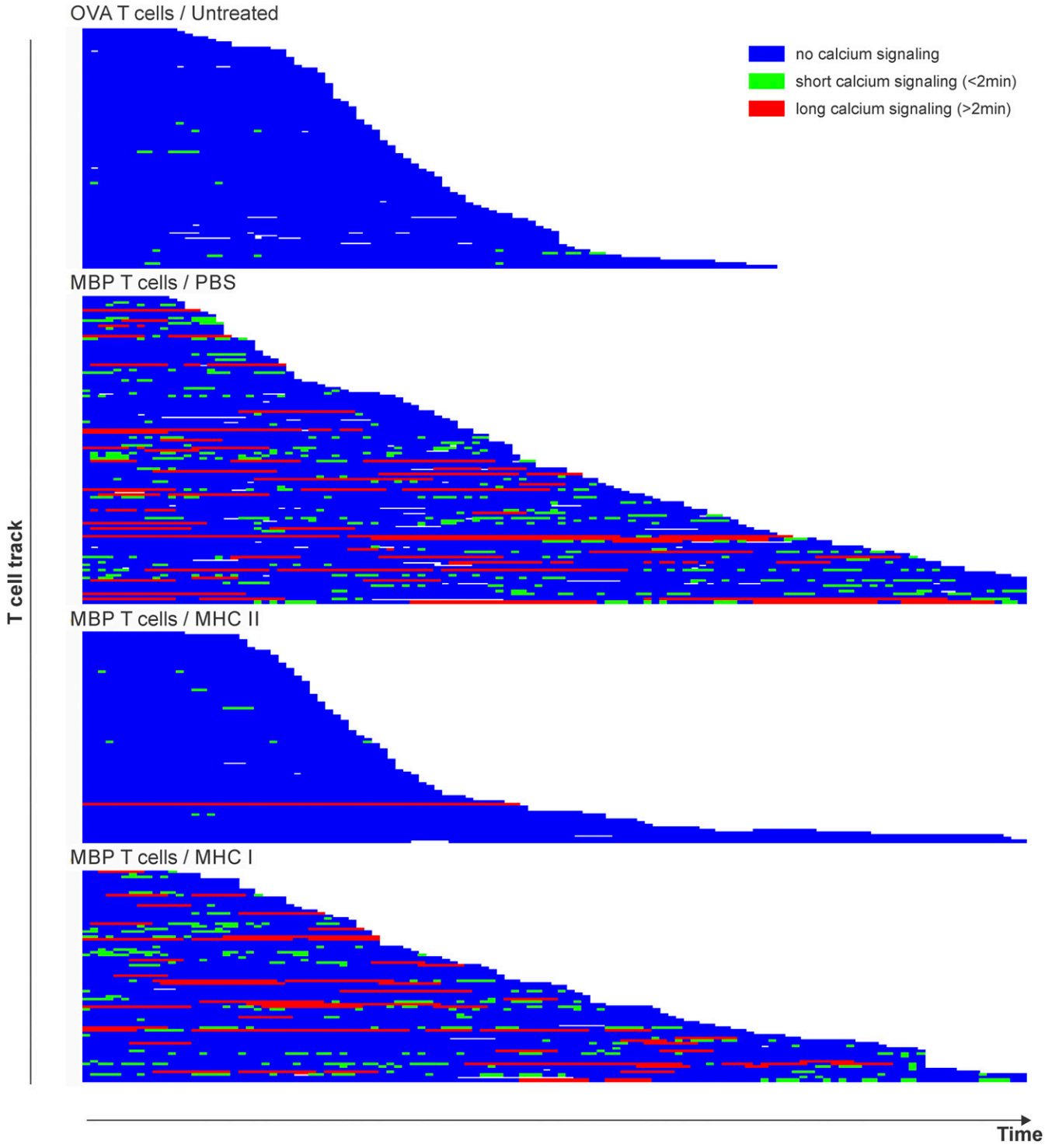

Fig. S3. Calcium signaling after MHC blocking. Calcium history plots of nontreated $T_{OVA\text{-}Twitch1}$ cells and $T_{MBP\text{-}Twitch1}$ cells on day 3 p.t. with or without antibody treatment. Each horizontal line represents one single T-cell track. In the calcium history plots, the blue color indicates low calcium levels, the green color indicates high calcium levels shorter than 2 min, and the red color indicates high calcium levels longer than 2 min.

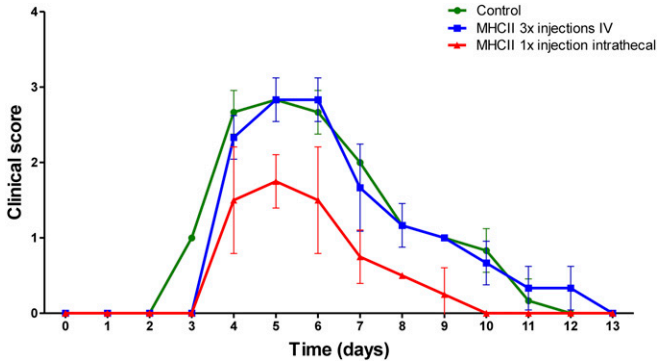

Fig. S4. Effect of anti-MHC class II antibody on clinical EAE. EAE clinical score after injection of anti-MHC class II antibody by i.v. or intrathecal injection. Representative results from at least three experiments are shown.

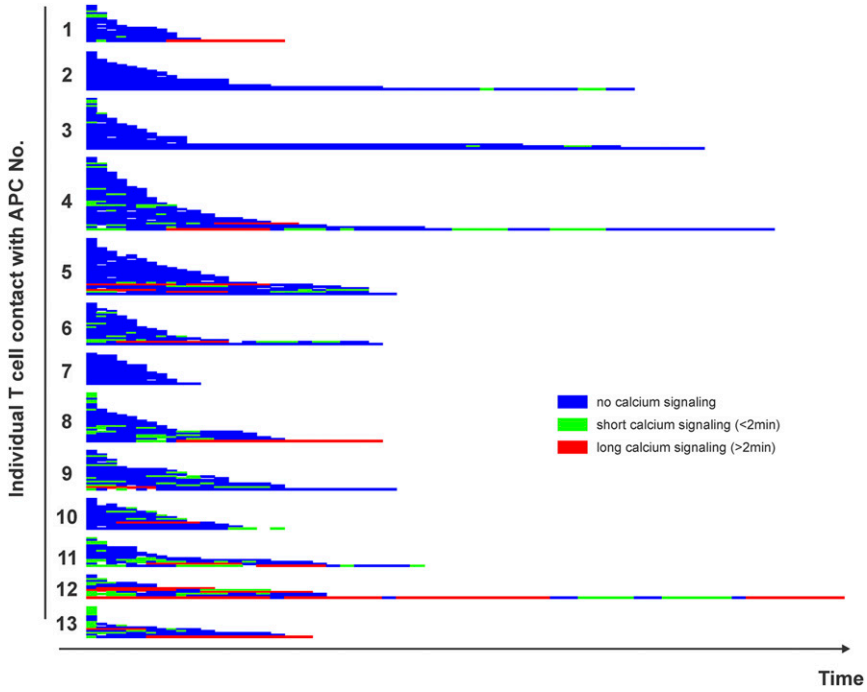

Fig. S5. Calcium history plot during contact with particular APCs. Calcium history plots of the $T_{MBP\text{-}Twitch1}$ cells during contact with APCs are shown. Numbers represent APCs identified in Fig. 6 *A*, *ii*. Each horizontal line represents a single continuous contact. Blue color indicates low calcium levels, green color indicates high calcium levels shorter than 2 min, and red color indicates high calcium levels longer than 2 min.

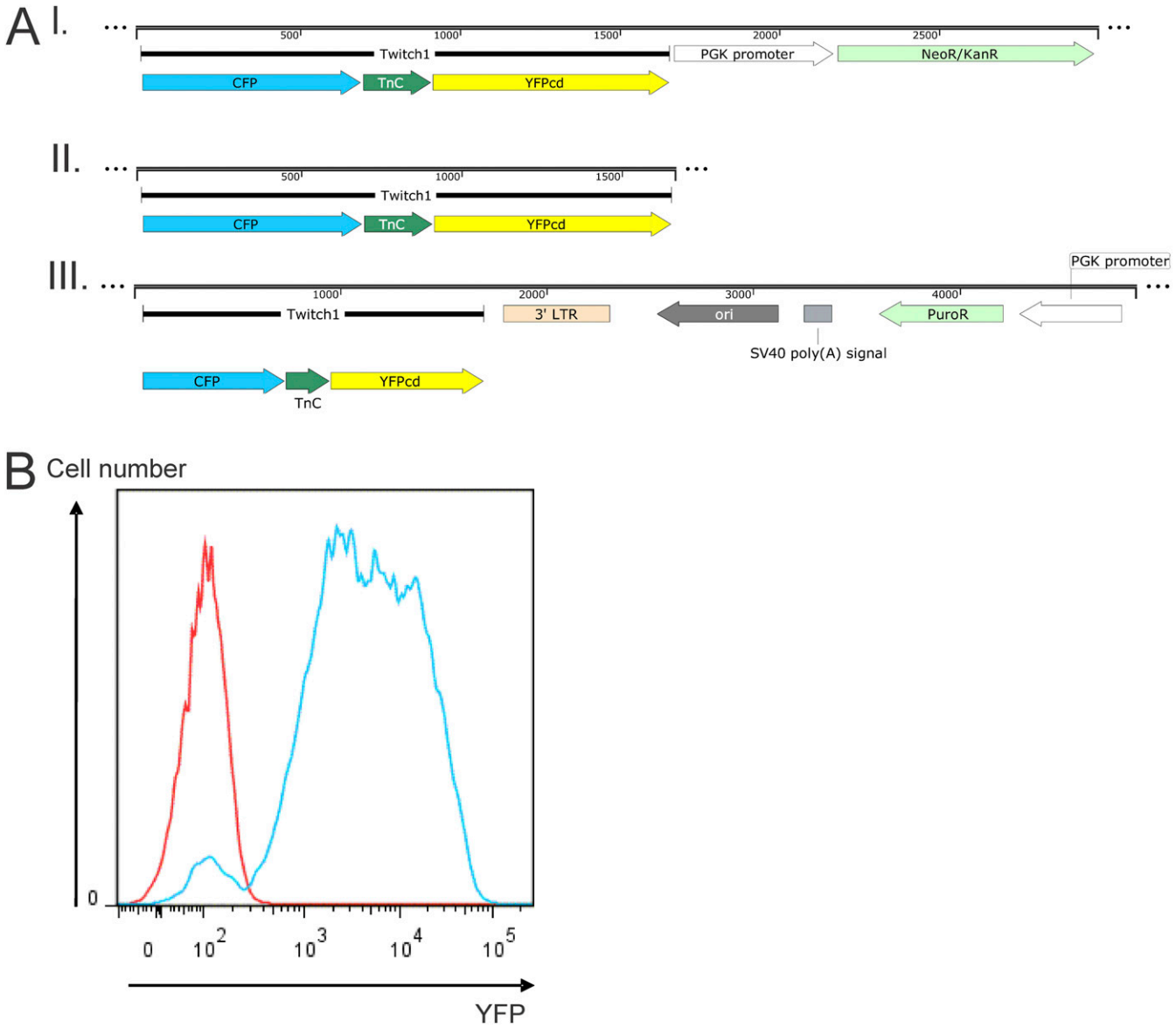

Fig. S6. Improved retroviral vector coding Twitch1. (*A*) Twitch1 retroviral constructs. The elements of each construct are shown here. (*I*) pMSCVneoTwitch1. (*II*) pMSCVΔneoTwitch1. (*III*) PINCOpuroTwitch1. Ori, origin of replication; puro, puromycin resistance gene. (*B*) Representative flow cytometric histogram depicting Twitch1 expression levels in $T_{MBP\text{-}Twitch1}$ (blue) and nonfluorescent MBP-specific T cells (red) at the seventh round of restimulation on day 2.

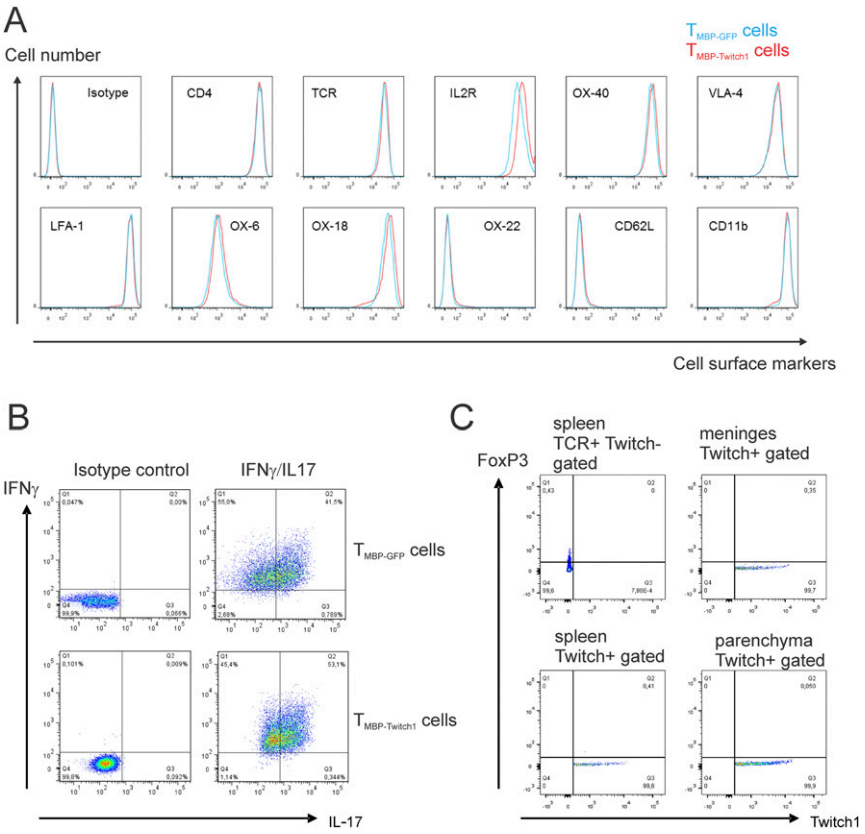

Fig. S7. Cellular phenotype of Twitch1-expressing T cells. (*A*) The phenotype of Twitch1-expressing T cells is compared with GFP-expressing T cells for cell surface markers (*A*) and the production of inflammatory cytokines (*B*). (*A*) The histograms depict the expression of cell surface markers on in vitro-activated GFP- or Twitch1-labeled T cells. $T_{MBP-GFP}$ (blue lines) and $T_{MBP-Twitch1}$ (red lines) cells were stained with specific antibodies as indicated and analyzed by flow cytometry. (*B*) Dot plots of IFNγ/IL-17 intracellular staining. The inserted numbers indicate the proportion of cells in each quadrant. Representative data from three independent experiments per cell line are shown. (*C*) Dot plots of Twitch1 expression and FoxP3 staining in ex vivo isolated T cells. Living cells were further gated as indicated. Representative result from two independent experiments including two rats per experiment is shown.

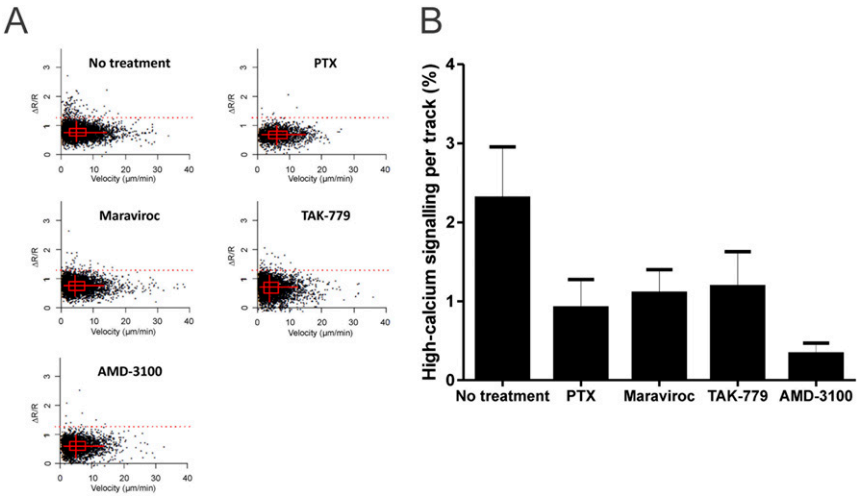

Fig. S8. Contribution of chemokine signaling to short-lived calcium signaling. (*A*) Scatterplots showing the $T_{OVA\text{-}Twitch1}$ velocity versus the calcium-indicator ratio change for each individual time point with or without inhibitor treatment. Mean values for ΔR/R and velocity are indicated along with a 2D box plot. The results are the sum of at least three independent experiments per treatment. (*B*) Percentage of high-calcium signaling per track in the spleen with or without inhibitor treatment.

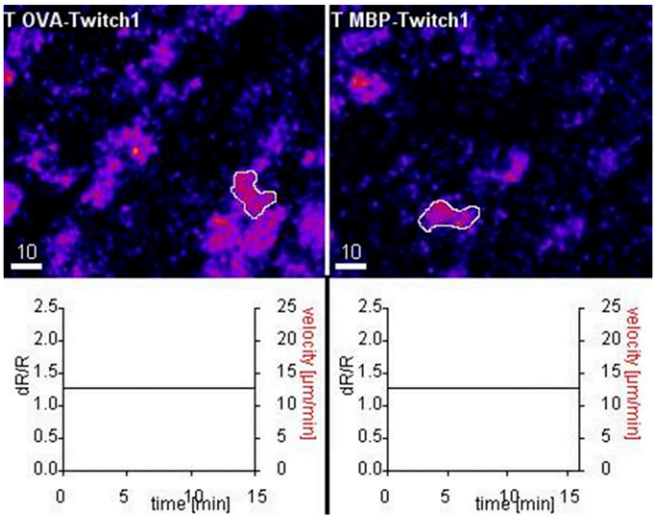

Movie S1. Short calcium signaling in spleen. $T_{OVA\text{-}Twitch1}$ cells (*Left*) and $T_{MBP\text{-}Twitch1}$ cells (*Right*) were imaged in the spleen on day 3 p.t. (*Upper*) Intracellular calcium level by pseudocolor ratio images. (*Lower*) Instantaneous velocity (red lines) and intracellular calcium levels as ΔR/R (black lines) at indicated time point. All movies run 10 frames per second (×250 speed).

Movie S1

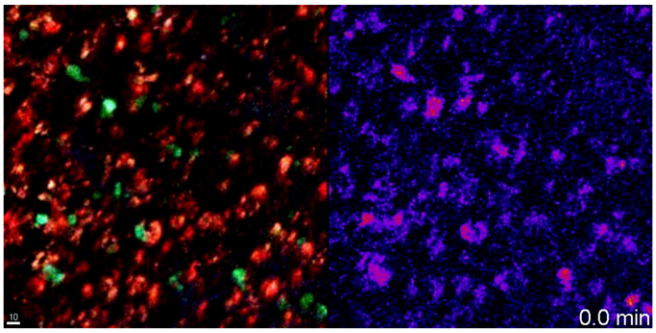

Movie S2. Visualization of calcium signaling in spleen before and after soluble MBP treatment. $T_{MBP\text{-}Twitch1}$ cells were imaged in spleen on day 3 p.t. A fluorescence overlay (*Left*) and a pseudocolor ratio image (*Right*) are depicted. Soluble MBP was injected at indicated time point. Blue/green, $T_{MBP\text{-}Twitch1}$ cells; red, splenic phagocytes visualized by detecting autofluorescence and i.v. infusion of fluorescent dextran at *Left*.

Movie S2

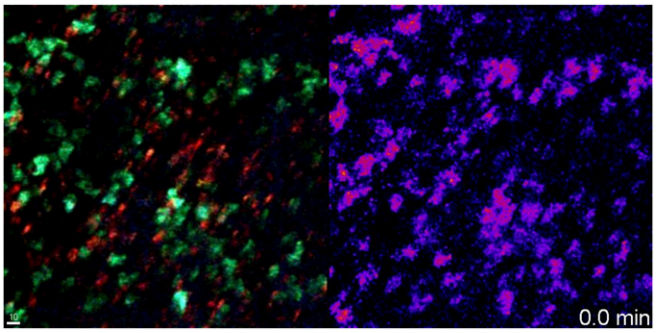

Movie S3. Visualization of calcium signaling in spleen before and after soluble OVA treatment. $T_{OVA\text{-}Twitch1}$ cells were imaged in spleen on day 3 p.t. A fluorescence overlay (*Left*) and a pseudocolor ratio image (*Right*) are depicted. Soluble OVA was injected at indicated time point. Blue/green, $T_{OVA\text{-}Twitch1}$ cells; red, splenic phagocytes visualized by detecting autofluorescence and i.v. infusion of fluorescent dextran at *Left*.

Movie S3

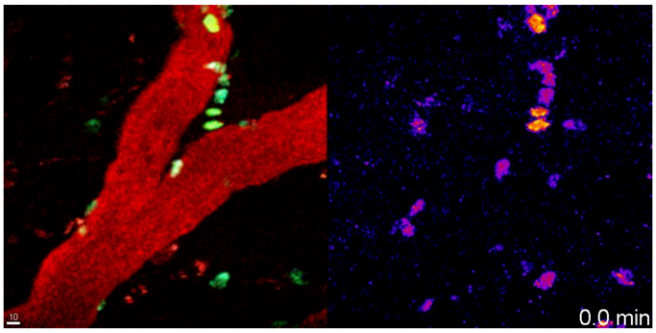

Movie S4. Visualization of calcium signaling of $T_{MBP\text{-}Twitch1}$ cells during the early prodromal phase of infiltration. $T_{MBP\text{-}Twitch1}$ cells were imaged in spinal cord leptomeninges on day 2 p.t. A fluorescence overlay (*Left*) and a pseudocolor ratio image (*Right*) are depicted. Blue/green, $T_{MBP\text{-}Twitch1}$ cells; red, blood vessels and phagocytes visualized by i.v. infusion of fluorescent dextran at *Left*.

Movie S4

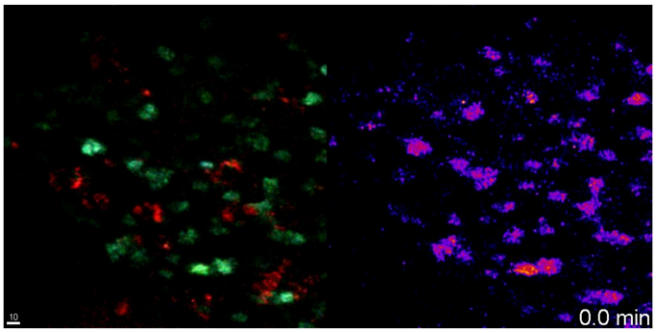

Movie S5. Calcium signaling of $T_{MBP\text{-}Twitch1}$ cells at leptomeninges after onset of EAE. $T_{MBP\text{-}Twitch1}$ cells were imaged in spinal cord leptomeninges on day 3 p.t. A fluorescence overlay (*Left*) and a pseudocolor ratio image (*Right*) are depicted. Blue/green, $T_{MBP\text{-}Twitch}$ cells; red, phagocytes visualized by intrathecal injection of fluorescent dextran at *Left*.

Movie S5

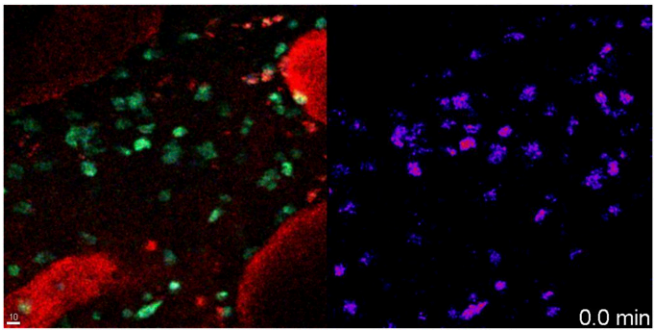

Movie S6. Calcium signaling of $T_{OVA\text{-}Twitch}$ cells at leptomeninges. $T_{OVA\text{-}Twitch1}$ cells were imaged in spinal cord leptomeninges on day 3 p.t. after cotransfer with nonlabeled MBP-specific T cells (not visible). A fluorescence overlay (*Left*) and a pseudocolor ratio image (*Right*) are depicted. Blue/green, $T_{OVA\text{-}Twitch1}$ cells; red, blood vessels and phagocytes visualized by i.v. and intrathecal injection of fluorescent dextran, respectively, at *Left*.

Movie S6

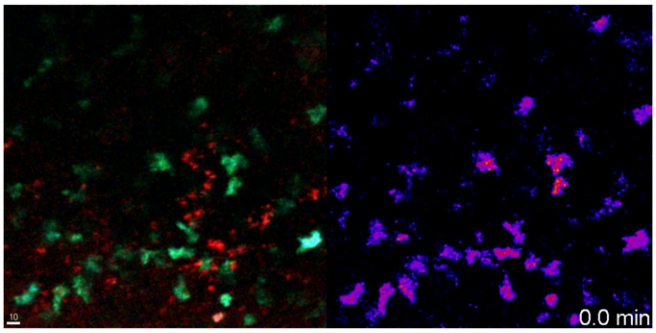

Movie S7. Calcium signaling of $T_{MBP\text{-}Twitch1}$ cells at leptomeninges after intrathecal injection of anti-MHC class II blocking antibody. $T_{MBP\text{-}Twitch1}$ cells were imaged in spinal cord leptomeninges on day 3 p.t. after intrathecal injection of anti-MHC class II blocking antibody. A fluorescence overlay (*Left*) and a pseudocolor ratio image (*Right*) are depicted. Blue/green, $T_{MBP\text{-}Twitch}$ cells; red, phagocytes visualized by intrathecal injection of fluorescent dextran at *Left*.

Movie S7

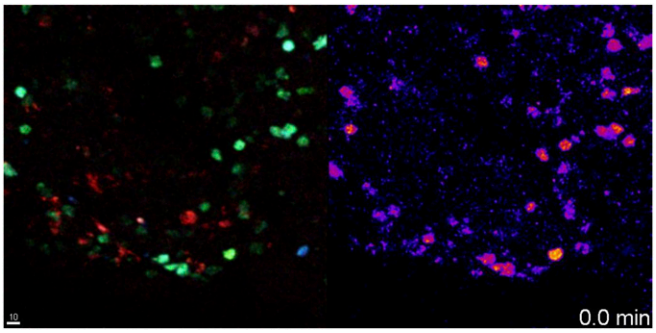

Movie S8. Calcium signaling of $T_{MBP\text{-}Twitch1}$ cells at leptomeninges after intrathecal injection of anti-MHC class I blocking antibody. $T_{MBP\text{-}Twitch1}$ cells were imaged in spinal cord leptomeninges on day 3 p.t. after intrathecal injection of anti-MHC class I blocking antibody. A fluorescence overlay (*Left*) and a pseudocolor ratio image (*Right*) are depicted. Blue/green, $T_{MBP\text{-}Twitch1}$ cells; red, phagocytes visualized by intrathecal injection of fluorescent dextran at *Left*.

Movie S8

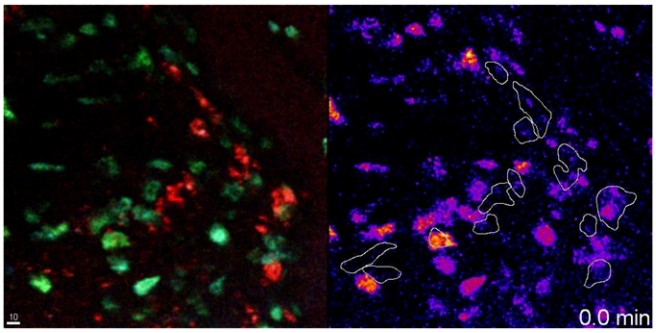

Movie S9. Antigen-presenting capacity of APCs at CNS leptomeninges. $T_{MBP\text{-}Twitch1}$ cells were imaged in spinal cord leptomeninges on day 3 p.t. A fluorescence overlay (*Left*) and a pseudocolor ratio image (*Right*) are depicted. Antigen-presenting cells are indicated with white lines at *Right*. Blue/green, $T_{MBP\text{-}Twitch1}$ cells; red, phagocytes visualized by intrathecal injection of fluorescent dextran at *Left*.

Movie S9